Neural transcription factor Pou4f1 promotes renal fibrosis via macrophage–myofibroblast transition

Patrick Ming-Kuen Tang[a,b,1,2], Ying-ying Zhang[b,c,1], Jun Xiao[b,1], Philip Chiu-Tsun Tang[a,1], Jeff Yat-Fai Chung[a], Jinhong Li[b], Vivian Weiwen Xue[a], Xiao-Ru Huang[b,d], Charing Ching-Ning Chong[e], Chi-Fai Ng[e], Tin-Lap Lee[f], Ka-Fai To[a], David J. Nikolic-Paterson[g], and Hui-Yao Lan[b,h,2]

[a]Department of Anatomical and Cellular Pathology, State Key Laboratory of Translational Oncology, Prince of Wales Hospital, The Chinese University of Hong Kong, 999077, Hong Kong; [b]Department of Medicine & Therapeutics, Li Ka Shing Institute of Health Sciences, Lui Che Woo Institute of Innovative Medicine, The Chinese University of Hong Kong, 999077, Hong Kong; [c]Department of Nephrology, Tongji Hospital, Tongji University School of Medicine, Shanghai, 200065, China; [d]Guangdong-Hong Kong Joint Laboratory on Immunological and Genetic Kidney Diseases, Guangdong Academy of Medical Sciences, Guangdong Provincial People's Hospital, Guangzhou, 510080, China; [e]SH Ho Urology Centre, Department of Surgery, The Chinese University of Hong Kong, 999077, Hong Kong; [f]Reproduction, Development and Endocrinology Program, School of Biomedical Sciences, The Chinese University of Hong Kong, 999077, Hong Kong; [g]Department of Nephrology and Monash University Department of Medicine, Monash Medical Centre, Clayton, VIC 3168, Australia; and [h]Guangdong-Hong Kong Joint Laboratory on Immunological and Genetic Kidney Diseases, The Chinese University of Hong Kong, 999077, Hong Kong

Edited by Richard Bucala, Yale University School of Medicine, New Haven, CT, and accepted by Editorial Board Member Carl F. Nathan July 13, 2020 (received for review October 9, 2019)

Unresolved inflammation can lead to tissue fibrosis and impaired organ function. Macrophage–myofibroblast transition (MMT) is one newly identified mechanism by which ongoing chronic inflammation causes progressive fibrosis in different forms of kidney disease. However, the mechanisms underlying MMT are still largely unknown. Here, we discovered a brain-specific homeobox/POU domain protein Pou4f1 (Brn3a) as a specific regulator of MMT. Interestingly, we found that Pou4f1 is highly expressed by macrophages undergoing MMT in sites of fibrosis in human and experimental kidney disease, identified by coexpression of the myofibroblast marker, α-SMA. Unexpectedly, Pou4f1 expression peaked in the early stage in renal fibrogenesis in vivo and during MMT of bone marrow-derived macrophages (BMDMs) in vitro. Mechanistically, chromatin immunoprecipitation (ChIP) assay identified that Pou4f1 is a Smad3 target and the key downstream regulator of MMT, while microarray analysis defined a Pou4f1-dependent fibrogenic gene network for promoting TGF-β1/Smad3-driven MMT in BMDMs at the transcriptional level. More importantly, using two mouse models of progressive renal interstitial fibrosis featuring the MMT process, we demonstrated that adoptive transfer of TGF-β1-stimulated BMDMs restored both MMT and renal fibrosis in macrophage-depleted mice, which was prevented by silencing Pou4f1 in transferred BMDMs. These findings establish a role for Pou4f1 in MMT and renal fibrosis and suggest that Pou4f1 may be a therapeutic target for chronic kidney disease with progressive renal fibrosis.

Pou4f1 | macrophage–myofibroblast transition | renal fibrosis

Fibrosis is a hallmark and common pathway leading to end-stage organ disease, including chronic kidney disease (CKD) (1). Myofibroblasts, a subset of activated fibroblasts characterized by expression of alpha-smooth muscle actin (α-SMA), are the principal cell type responsible for the synthesis and deposition of fibrillar collagen deposition during tissue fibrosis (2). Myofibroblasts are a heterogeneous population which can arise from a number of sources (3), including epithelial–mesenchymal transition (4, 5), endothelial–mesenchymal transition (6), proliferation of local resident fibroblasts and pericytes (6), and from the bone marrow (7–10). The origin of myofibroblasts during renal fibrosis remains controversial and a better understanding of these processes may uncover new therapeutic targets for fibrotic kidney disease.

Increasing evidence shows that active and unresolving inflammation may lead to the development of progressive renal fibrosis which is associated with the process of macrophage–myofibroblast transition (MMT) as reported in both human and experimental animal models (7–18). Indeed, macrophages and myofibroblasts are present in active fibrotic lesions and MMT cells are identified by coexpression of both macrophage (e.g., CD68 and F4/80) and myofibroblast (α-SMA) markers. Our studies have identified that MMT is an important pathway contributing to a substantial proportion of α-SMA$^+$ myofibroblasts in active fibrotic lesions in both human and experimental kidney disease, including inflammatory forms of glomerulonephritis and chronic renal allograft rejection (11–15). MMT cells are prominent in areas with active fibrotic lesions, but are absent or rare in normal kidney or kidney with acute inflammation (14), suggesting that MMT is an important mechanism by which chronic inflammation leads to progressive fibrosis (15). These findings are supported by studies from other groups showing that labeled bone marrow cells transition into α-SMA$^+$ myofibroblasts in models of renal fibrosis (7, 8, 16–18).

TGF-β/Smad signaling is recognized as the master regulator of tissue fibrosis (19). Both the process of MMT and the development of renal fibrosis are tightly regulated by Smad3, but not Smad2 (13). As systemic inhibition of Smad3 may induce autoimmune

Significance

Macrophage–myofibroblast transition (MMT) is a newly discovered pathogenic process by which TGF-β1/Smad3 signaling promotes tissue scarring. However, systemic targeting of Smad3 may impair host T cell immunity; therefore, it is preferable to focus on downstream mechanisms to identify antifibrotic therapies that avoid targeting Smad3 per se. In this study, we revealed a brain-specific transcription factor Pou4f1 as the key regulator by which TGF-β1/Smad3 signaling executes MMT. Macrophage-specific silencing of Pou4f1 effectively blocked progression of renal fibrosis in two mouse kidney disease models. Thus, Pou4f1 represents a therapeutic target in MMT-driven renal diseases.

Author contributions: P.M.-K.T., Y.-y.Z., and H.-Y.L. designed research; P.M.-K.T., Y.-y.Z., J.X., P.C.-T.T., J.Y.-F.C., J.L., and X.-R.H. performed research; P.M.-K.T., C.C.-N.C., C.-F.N., T.-L.L., and K.-F.T. contributed new reagents/analytic tools; P.M.-K.T., V.W.X., T.-L.L., and D.J.N.-P. analyzed data; and P.M.-K.T., Y.-y.Z., D.J.N.-P., and H.-Y.L. wrote the paper.

The authors declare no competing interest.

This article is a PNAS Direct Submission. R.B. is a guest editor invited by the Editorial Board.

[1]P.M.-K.T., Y.-y.Z., J.X., and P.C.-T.T. contributed equally to this work.

[2]To whom correspondence may be addressed. Email: patrick.tang@cuhk.edu.hk or hylan@cuhk.edu.hk.

This article contains supporting information online at https://www.pnas.org/lookup/suppl/doi:10.1073/pnas.1917663117/-/DCSupplemental.

First published August 11, 2020.

disease by impairing the host immune system (20), it is important to look for alternative therapeutic targets downstream of TGF-β/Smad3 signaling. High-throughput RNA sequencing (RNA-seq) has revealed a number of Smad3-dependent lncRNAs that are associated with kidney injury (21–23). In addition, we have employed single-cell RNA-seq in an in vitro model of MMT to identify Smad3-dependent MMT transcriptomes (24). Using unbiased gene network analysis, the neuron-specific transcription factor, Pou4f1 (Brn3a) (25), was predicted as the only transcription factor involved in MMT (24). This was an unexpected finding as Pou4f1 is expressed in the developing peripheral sensory nervous system, retinal ganglion cells, and lymphocytic lineage cells; however, its role in kidney disease is unknown.

Based on these findings, we hypothesize that Pou4f1 plays a central regulatory role in TGF-β1/Smad3-mediated MMT. Here, we show that Pou4f1 expression is increased in human kidney disease with active fibrotic lesions, as well as being up-regulated in two experimental models of renal fibrosis: unilateral ureteral obstruction (UUO) and renal ischemia/reperfusion injury (IRI). In particular, Pou4f1 is expressed by kidney-infiltrating macrophages in progressive renal fibrosis, with the proportion of Pou4f1$^+$ macrophages correlating with the degree of MMT in human kidney tissues. Mechanistically, we demonstrated that Smad3 binds to the Pou4f1 gene promoter and enhances Pou4f1 gene transcription. In addition, we identified a profibrogenic network by which Pou4f1 promotes TGF-β1/Smad3-driven MMT in vitro. Finally, using adoptive transfer in UUO and IRI models, we established that silencing of Pou4f1 in bone marrow-derived macrophages (BMDMs) prevents infiltrating kidney macrophages from undergoing MMT, resulting in a substantial reduction in renal fibrosis. Thus, Pou4f1 represents a therapeutic target in MMT-driven tissue fibrosis.

Results

Pou4f1 Markedly Increases in Injured Kidney Associated with Renal Fibrosis. To examine the involvement of Pou4f1 in renal pathogenesis, we investigated Pou4f1 expression in human kidney

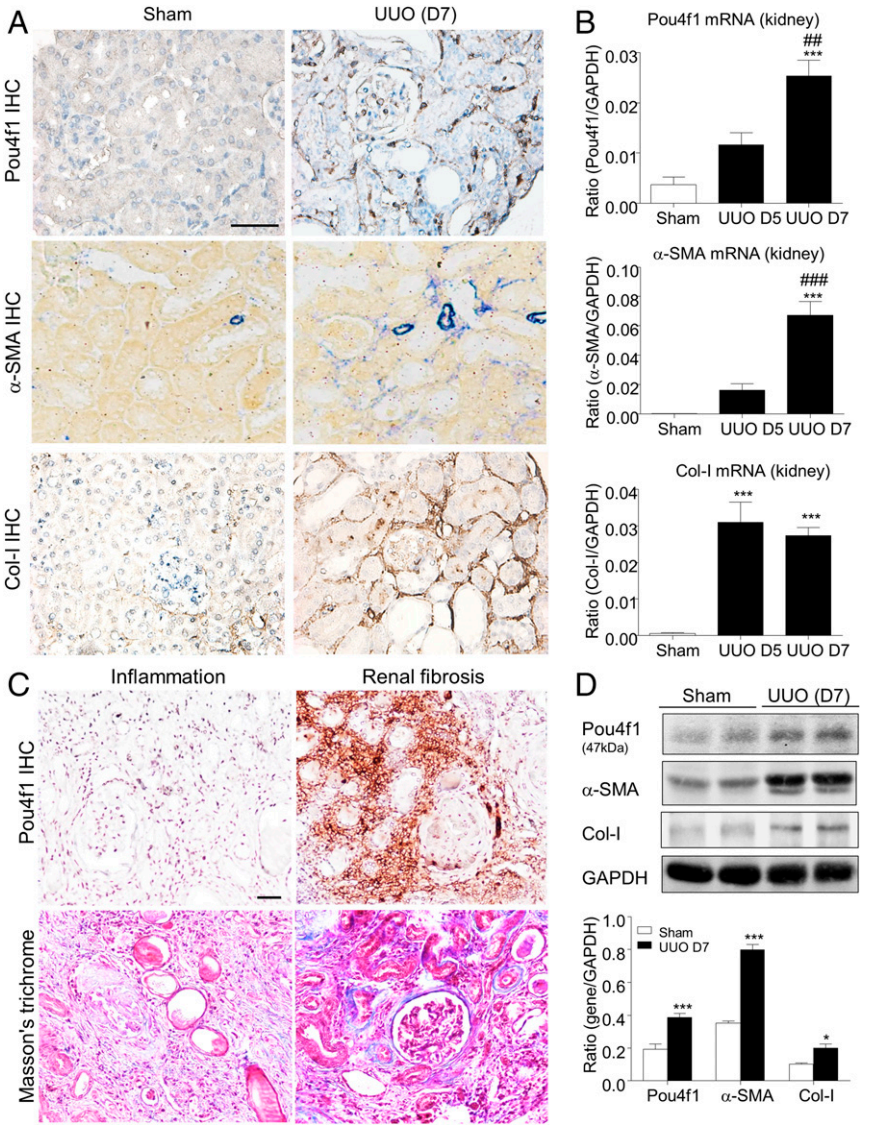

Fig. 1. Pou4f1 is expressed in the fibrosing kidney. Pou4f1 expression by interstitial cells in the UUO kidney is associated with markers of renal fibrosis; α-SMA and collagen I (Col-I), compared to the sham control as shown by (*A*) immunostaining, and (*B*) real-time PCR. (*C*) Immunostaining in a case of human chronic allograft nephropathy shows Pou4f1 expression in many interstitial cells in an area of active fibrosis (*Right*), whereas little Pou4f1 staining is seen in a different area with severe inflammation only (*Left*). Lesions are also shown by Masson's trichrome staining. (*D*) Western blot shows increased levels of Pou4f1 and fibrotic markers on day 7 UUO. Data represent results from eight mice/group. (*B*) $^*P < 0.05$, $^{***}P < 0.001$ vs. sham control; $^{\#\#}P < 0.01$, $^{\#\#\#}P < 0.001$ vs. UUO day 5; (*C*) $^{***}P < 0.001$ vs. day 7 sham. (Scale bars, 50 μm.)

disease and in the mouse UUO model (22, 24). We found that Pou4f1 was expressed at low levels in normal mouse kidney, but was strongly expressed by kidney-infiltrating cells in the UUO kidney in association with up-regulation of fibrosis markers α-SMA and collagen I (Fig. 1*A*). Analysis of days 5 and 7 in the UUO model found that the pattern of increasing levels of Pou4f1 mRNA levels closely followed that of the myofibroblast marker α-SMA (Fig. 1*B*). Up-regulation of Pou4f1 in the UUO model was confirmed by Western blotting (Fig. 1*D*). We demonstrated strong up-regulation of Pou4f1 in a case of chronic allograft dysfunction (CAD) with a dense infiltration of Pou4f1$^+$ cells in an area with active fibrosis, whereas an area in the same tissue featuring inflammation only lacked Pou4f1$^+$ cells (Fig. 1*C*).

Pou4f1 Peaks at the Early Phase of Fibrogenesis in the Renal MMT Cells. In contrast to mRNA levels, Western blotting showed that protein levels of Pou4f1 peaked on day 5 in the UUO model which occurred prior to the peak of myofibroblast marker α-SMA and collagen I protein expression (Fig. 2*A* and *SI Appendix*, Fig. S1). The peak of Pou4f1 mRNA on day 5 of UUO also preceded the peak of the macrophage infiltrate, assessed using the F4/80 marker, indicating that Pou4f1 induction occurs soon after macrophages infiltrate the injured kidney (Fig. 1*B* and *SI Appendix*, Fig. S1).

Our unbiased gene network analysis predicted that Pou4f1 is the only transcription factor involved in MMT (24), leading us to examined its expression in kidney-infiltrating macrophages. Flow cytometric analysis of enzyme-digested tissue revealed a population of Pou4f1-expressing macrophages (Pou4f1$^+$F4/80$^+$ cells) and Pou4f1-expressing MMT (α-SMA$^+$F4/80$^+$) cells in the day 7 UUO kidney (Fig. 2*B*). This was confirmed by three-color confocal microscopy which identified Pou4f1 expression by MMT (α-SMA$^+$F4/80$^+$) cells in the UUO kidney (Fig. 2*C*). This was quantified by flow cytometry in which F4/80$^+$ macrophages were gated into Pou4f1$^+$ and Pou4f1$^-$ populations and analyzed for α-SMA expression and showed that more than 60% of α-SMA$^+$F4/80$^+$ MMT cells expressed Pou4f1 in day 5 UUO kidney (Fig. 2*D* and *SI Appendix*, Fig. S2). Importantly, coexpression of Pou4f1 and the MMT marker α-SMA$^+$ was confirmed in infiltrating CD68$^+$ macrophages (>25%) in a single case of CAD with renal fibrosis using flow cytometry analysis (Fig. 2*E* and *SI Appendix*, Fig. S2). Our findings imply that Pou4f1 may facilitate the transition of renal inflammation into renal fibrosis via promoting MMT in the injured kidney.

Pou4f1 Correlates with MMT in Human Kidney Disease. In human kidney disease, immunostaining for CD68 and α-SMA found a substantial population of α-SMA$^+$CD68$^+$ (yellow) cells in lesions of interstitial fibrosis/tubular atrophy in a case of CAD, whereas few or no MMT cells were seen in cases of diabetic kidney disease (DKD) and end-stage renal disease (ESRD) which lacked active fibrosis (Fig. 3*A*). Three-color staining in CAD showed Pou4f1 expression by α-SMA$^+$CD68$^+$ MMT cells, which is evident as the white cells in the three-dimensional (3D) image in Fig. 3*B*. Analysis of the staining showed a considerable population of α-SMA$^+$CD68$^+$ MMT cells in both CAD and ESRD, with MMT cells making a substantial contribution to the total α-SMA$^+$ myofibroblast population, particularly in CAD, while little MMT was seen in DKD (Fig. 3*C*). A highly significant P value ($P < 0.0001$) was evident between Pou4f1$^+$ macrophages and the proportion of MMT cells in the total α-SMA$^+$ myofibroblast population across the different types of kidney disease (Fig. 3*C* and Dataset S1). These findings imply a role for Pou4f1 in MMT-driven renal fibrosis.

Pou4f1 Is a Smad3 Target Gene during TGF-β1-Driven MMT. Unbiased gene analysis predicted Pou4f1 as the only transcription factor in the key regulatory network of TGF-β1/Smad3-induced MMT in BMDMs in our previous work (24). Here, we hypothesized that Pou4f1 is tightly regulated by Smad3 and further investigated the underlying mechanisms in vivo and in vitro. In wild-type mice (Smad3-WT), many Pou4f1$^+$ interstitial cells were evident in the day 7 UUO kidney; however, mice lacking Smad3 (Smad3-knockout [KO]) showed a marked reduction in Pou4f1$^+$ interstitial cells on day 7 UUO (Fig. 4*A*). This was confirmed by a marked reduction in Pou4f1 mRNA levels in the Smad3-KO UUO kidney in vivo (Fig. 4*B*).

In addition, Pou4f1 mRNA levels were substantially reduced in Smad3-KO versus Smad3-WT BMDMs following TGF-β1 stimulation in vitro (Fig. 4*C*). A 24-h stimulation with TGF-β1 induces up-regulation of Pou4f1 mRNA levels in BMDMs which can be prevented by inhibiting our previous identified MMT regulator Src kinase (24), while Pou4f1 mRNA levels are dramatically reduced by inactivating Smad3 with the specific inhibitor SIS3 (*SI Appendix*, Fig. S3). At the transcriptional level, we identified a conserved Smad3 binding site in the promoter region of human and murine Pou4f1 genomic sequences (Fig. 4*D*). Using chromatin immunoprecipitation (ChIP) assays, we confirmed that TGF-β1 stimulation of BMDMs significantly enriched the binding of Smad3 on the predicted Pou4f1 promoter sequence (Fig. 4*E*). In addition, a dual reporter assay demonstrated that Smad3-mediated Pou4f1 transcription was blocked by deletion of the Smad3 binding site (Pou4f1-mutant) or by mutation of the Smad3 phosphorylation site (Smad3-mutant) (Fig. 4*F* and *SI Appendix*, Fig. S4). These findings identify that Pou4f1 is tightly regulated by Smad3 at the transcriptional level during TGF-β1-induced MMT.

Pou4f1 Promotes MMT-Mediated Tissue Fibrosis via a Fibrogenic Gene Network. To investigate the functional role of Pou4f1 in MMT, we examined the time course of Pou4f1 expression in cultured BMDMs undergoing TGF-β1-driven MMT in vitro. Interestingly, TGF-β1 (5 ng/mL) transiently increased Pou4f1 mRNA levels at day 1 in BMDMs, which rapidly returned to basal levels afterward (Fig. 5*A*). Similarly, Pou4f1 protein levels also peaked at 24 h after TGF-β1 stimulation of BMDMs, which preceded the peak of α-SMA and collagen I protein expression on day 5 (Fig. 5*B*). By contrast, short-term stimulation with classic inflammatory factors IL-1β and LPS did not trigger Pou4f1 expression in BMDMs (*SI Appendix*, Fig. S5), consistent with the lack of Pou4f1 staining in areas of active inflammation without fibrosis (Fig. 1*C*). Moreover, the use of siRNA to silence Pou4f1 expression in BMDMs was highly effective in suppressing TGF-β1-induced MMT. This was shown by preventing α-SMA expression and development of an elongated morphology in BMDMs on day 5 after TGF-β1 stimulation (Fig. 5*C*) and by Western blotting showing reduced α-SMA and collagen I protein levels (Fig. 5*D*).

To investigate the role of Pou4f1 in tissue fibrosis, we compared the transcriptome profiles of Pou4f1-silenced (siPou4f1) or nonsense siRNA-treated (NC) BMDMs undergoing TGF-β1-driven MMT. In brief, both NC-BMDMs and siPou4f1-BMDMs were cultured with or without 5 ng/mL of TGF-β1 for 24 h. The reported downstream proteins of Pou4f1 related to actin formation were significantly down-regulated in TGF-β1-stimulated BMDMs by Pou4f1-knockdown in vitro at 24 h (*SI Appendix*, Fig. S6). In order to identify the Pou4f1-specific target genes that promote MMT, these samples were submitted for further analysis with Affymetrix GeneChip mouse gene 2.1 ST array. The results showed transcriptome profiles that were readily distinguished between the conditions (Fig. 5 *E* and *F*). In particular, we identified 215 differentially expressed genes (DEGs) that were specifically related to TGF-β1-driven MMT on day 1, of which 51 genes were regulated in a Pou4f1-dependent manner (Fig. 5*G*, *SI Appendix*, Fig. S7, and Dataset S2). Surprisingly, unbiased gene network analysis reconstructed a fibrogenic gene network using the Pou4f1-dependent genes (Fig. 5*H*). Our findings identified a pathogenic role of Pou4f1 in MMT by facilitating TGF-β1/Smad3-driven

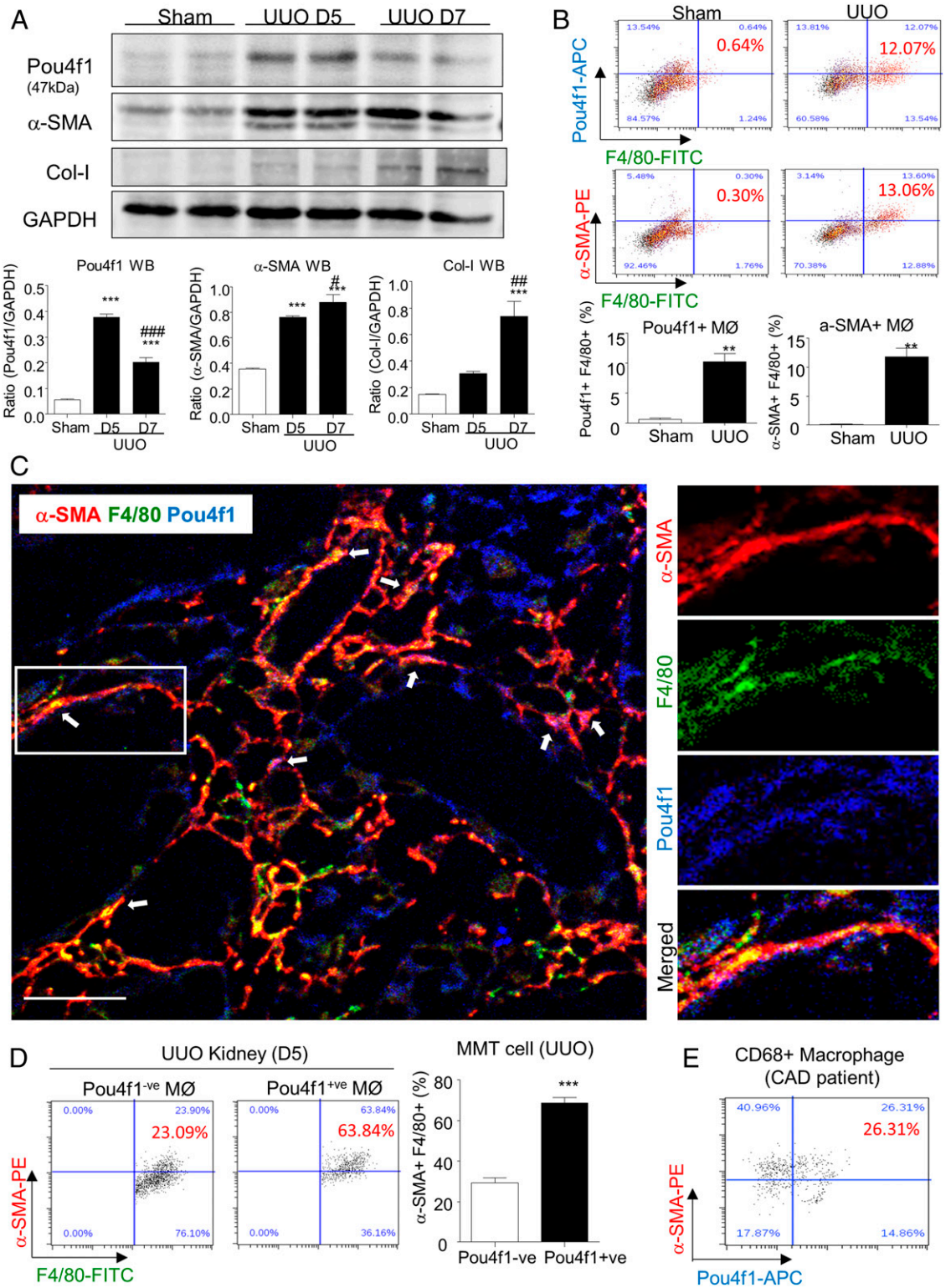

Fig. 2. Pou4f1 is expressed by MMT cells in the UUO model. (*A*) Western blot analysis shows increased Pou4f1 expression on days 5 and 7 UUO in association with increased levels of the myofibroblast marker α-SMA and collagen I (Col-I). Graphs show quantification of the blots. (*B*) Flow cytometry analysis of kidney samples derived by enzyme digestion. The plots show double staining for Pou4f1 with F4/80 or α-SMA. Graphs show the percentage of $F4/80^+$ cells and $\alpha\text{-SMA}^+$ cells that coexpress Pou4f1. (*C*) Confocal microscopy with z-stack scanning identified Pou4f1 (blue) expression by MMT cells (α-SMA, red; F4/80, green) in the day 7 UUO kidney. (*D*) Flow cytometric analysis of day 5 UUO kidney showing α-SMA expression by $Pou4f1^+F4/80^+$ and $Pou4f1^-F4/80^+$ cells. Graph shows the percentage of MMT cells ($\alpha\text{-SMA}^+F4/80^+$ cells) that coexpress Pou4f1 on day 5 UUO. (*E*) Flow cytometric analysis of double staining for Pou4f1 and α-SMA in a single kidney sample from a patient with chronic allograft dysfunction (CAD). Data represent results from eight mice/group. (*A* and *B*) $^{**}P < 0.01$, $^{***}P < 0.001$ vs. sham control; $^{\#}P < 0.05$, $^{\#\#}P < 0.01$, $^{\#\#\#}P < 0.001$ vs. D5 UUO kidney; (*D*) $^{***}P < 0.001$ vs. $Pou4f1^{-ve}$ macrophages. (Scale bars, 50 μm.)

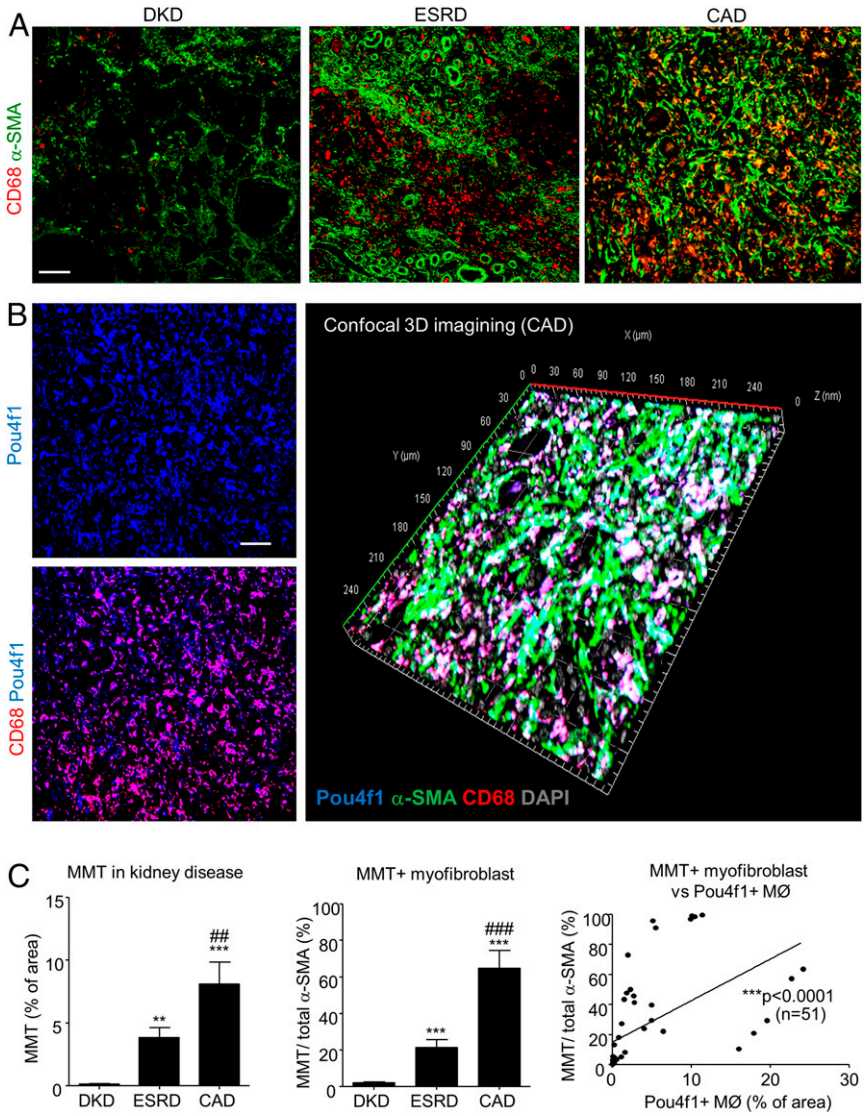

Fig. 3. Pou4f1 is expressed by MMT cells in human kidney disease. (*A*) Confocal microscopy shows that CD68$^+$ macrophages (red) and α-SMA$^+$ myofibroblasts (green) are distinct cell populations in cases of end-stage renal disease (ESRD) and diabetic kidney disease (DKD). By contrast, many MMT cells coexpressing CD68 and α-SMA (yellow) can be seen in an area of active fibrosis in a case of chronic allograft dysfunction (CAD). (*B*) Opal multiplex IHC system identified that most CD68$^+$ macrophages express Pou4f1 (purple) in an area of active fibrosis in CAD, including Pou4f1 expression by many α-SMA$^+$CD68$^+$ MMT cells (white). This is more clearly seen in the 3D illustration. (*C*) Graphs show quantification of staining from a cohort of 10 cases of kidney disease. A significant correlation is evident between Pou4f1$^+$ macrophages and the contribution of the MMT cells in total α-SMA$^+$ myofibroblasts. (*C*) $^*P < 0.05$, $^{**}P < 0.01$, $^{***}P < 0.001$ vs. ESRD; $^{\#\#}P < 0.001$, $^{\#\#\#}P < 0.001$ vs. ESRD. (Scale bars, 100 μm.)

renal fibrosis, which may represent a precise therapeutic target for MMT-driven tissue scarring.

Silencing of Pou4f1 Blocks MMT-Driven Renal Fibrosis in a Mouse Model of UUO. To investigate the function of Pou4f1 in MMT and renal fibrosis in vivo, we used adoptive transfer of BMDMs in the UUO model under macrophage depletion. To deplete endogenous macrophages, LysM-Cre/diphtheria toxin receptor (DTR) mice were treated with diphtheria toxin (DT) for 3 d prior to UUO surgery (14, 26). Mice then received an injection of Pou4f1-silenced (siPou4f1) or nonsense siRNA-treated (NC) BMDMs which had been stimulated with TGF-β1 for 24 h before transfer. In the absence of macrophage depletion, immunostaining and flow cytometry showed the presence of many interstitial Pou4f1$^+$ cells in the day 5 UUO kidney, along with many α-SMA$^+$ myofibroblasts and F4/80$^+$ macrophages, including a substantial population of α-SMA$^+$F4/80$^+$ MMT cells (Fig. 6 *A* and *B*). This was accompanied by renal fibrosis as shown by increased levels of collagen I in the day 5 UUO kidney and increases in α-SMA mRNA and protein levels (Fig. 7 *A*–*C*). By contrast, DT-based macrophage depletion without adoptive transfer showed a marked reduction in Pou4f1$^+$ cells and F4/80$^+$ macrophages, with a partial reduction in α-SMA$^+$ myofibroblasts, and very few α-SMA$^+$F4/80$^+$ MMT cells (Fig. 6 *A* and *B*). This was associated with a significant reduction in renal fibrosis in terms of collagen I deposition and α-SMA protein and mRNA levels (Fig. 7 *A*–*C*). However, transfer of NC-BMDMs into DT-treated mice restored the F4/80 macrophage population; this also restored Pou4f1$^+$ interstitial cells, α-SMA$^+$ myofibroblasts, α-SMA$^+$F/80$^+$ MMT cells, and the full development of renal fibrosis (Figs. 6 *A* and *B* and 7 *A*–*C*). The transfer of siPou4f1-BMDM into DT-treated mice restored the kidney F4/80$^+$ macrophage population,

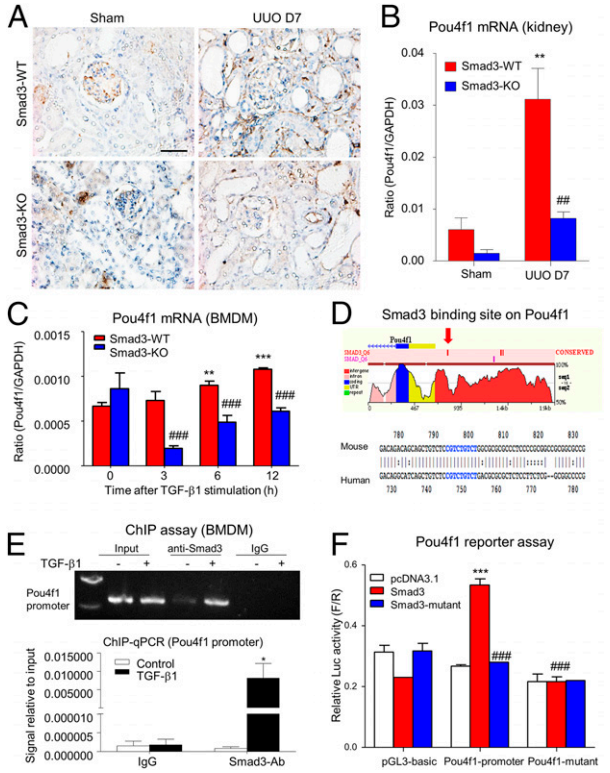

Fig. 4. Pou4f1 expression is tightly regulated by Smad3 in MMT cells in vivo and in vitro. (*A*) Immunostaining shows many Pou4f1$^+$ interstitial cells in the day 7 UUO kidney in wild-type mice (Smad3-WT), which were markedly reduced in the UUO kidney in mice lacking Smad3 (Smad3-KO). (*B*) Similarly, Pou4f1 mRNA levels were substantially increased in day 7 UUO kidney in Smad3-WT mice and reduced in day 7 UUO Smad3-KO mice. (*C*) Time course of TGF-β1 stimulation of cultured BMDMs shows increased Pou4f1 mRNA in Smad3-WT cells, but not in Smad3-KO cells. (*D*) A conserved Smad3 binding site (red narrow) is evident in the promoter region of the human and mouse Pou4f1 genomic sequence by ECR browser. (*E*) TGF-β1 stimulation of BMDMs significantly enriched physical binding of the Smad3 protein to the Pou4f1 promoter region as shown by ChIP and ChIP-PCR assays. (*F*) The Smad3 binding site, but not a mutated Smad3 binding site, induced transcription of Pou4f1 in a dual-luciferase assay. Data represent three independent in vitro experiments or from eight mice/group. (*B* and *C*) $^{**}P < 0.01$, $^{***}P < 0.001$ vs. sham or control; $^{\#\#}P < 0.01$, $^{\#\#\#}P < 0.001$ vs. Smad3-WT; (*E*) $^{*}P < 0.05$ vs. TGF-β1-stimulated IgG; (*F*) $^{***}P < 0.001$ vs. pcDNA3.1, $^{\#\#\#}P < 0.001$ vs. Smad3-expressed Pou4f1-promoter group. (Scale bars, 50 μm.)

but not the interstitial Pou4f1$^+$ cells, α-SMA$^+$ myofibroblasts, or α-SMA$^+$F4/80$^+$ MMT cells (Fig. 6 *A* and *B*) and failed to promote the fibrogenesis (Fig. 7 *A*–*C*). This demonstrates an essential role for Pou4f1 in MMT-mediated renal fibrosis in vivo.

Silencing of Pou4f1 Blocks MMT-Driven Renal Fibrosis in a Mouse Model of IRI. To further confirm the key role of Pou4f1 in mediating MMT and renal fibrosis, we employed the macrophage adoptive transfer approach in a second model of renal fibrosis induced by IRI. Macrophage depletion was conducted on LysM-Cre/DTR mice with DT for 3 d prior to IRI surgery, followed by adoptive transferring of siPou4f1-BMDM or NC-BMDM on day 1 and then killed on day 7. In the absence of macrophage depletion, the IRI kidney exhibited many interstitial Pou4f1$^+$ cells, F4/80$^+$ macrophages, α-SMA$^+$ myofibroblasts, and a clear population of α-SMA$^+$F4/80$^+$ MMT cells together with renal fibrosis as shown by deposition of collagen I (Fig. 8 *A*–*C*). In contrast, DT-mediated macrophage depletion largely abrogated F4/80$^+$ macrophages, substantially reduced Pou4f1 expression, with few α-SMA$^+$F4/80$^+$ MMT cells evident, and resulted in a significant reduction in α-SMA$^+$ myofibroblasts and collagen I deposition (Fig. 8 and *SI Appendix*, Fig. S8). Adoptive transfer with NC-BMDM restored F4/80$^+$ macrophages, Pou4f1$^+$ cells, Pou4f1$^+$CD68$^+$ macrophages, and α-SMA$^+$F4/80$^+$ MMT cell populations as well as restoring renal fibrosis (Fig. 8 and *SI Appendix*, Fig. S8). By contrast, transfer of siPou4f1-BMDM restored the kidney F4/80$^+$ macrophage population, but failed to restore Pou4f1 expression, MMT cells, α-SMA$^+$ myofibroblasts, or renal fibrosis (Fig. 8 and *SI Appendix*, Fig. S8). Our results clearly demonstrated the pathogenic role of Pou4f1 in renal fibrosis and suggest it represents a therapeutic target for preventing MMT-driven kidney diseases.

Discussion

TGF-β/Smad3 signaling is a master regulator of tissue fibrosis; however, TGF-β1 and Smad3 also play important roles in regulating the immune response; thus we need to look downstream of TGF-β and Smad3 for potential therapeutic targets to intervene in chronic fibrotic disease (19). Our previous study revealed an important role for TGF-β1/Smad3-dependent MMT in human and experimental kidney fibrosis (13, 15, 24). Using single-cell RNA sequencing in TGF-β1-stimulated Smad3-WT and Smad3-KO BMDMs, we uncovered a Src-centric gene network as a key event in the MMT process (24). Src is a nonreceptor tyrosine kinase that is involved in many signaling pathways (27), leading us to look for downstream transcription factors that might be responsible for orchestrating MMT. Notably, we identified that Pou4f1, a brain-specific homeobox/POU domain protein (25), was the only transcription factor in the Src-centric MMT-dependent regulatory gene network (24). In this study, we provide evidence that Pou4f1 regulates MMT and renal fibrosis in vitro and in vivo.

Pou4f1 is documented as a transcription factor involved in neuron development (25), although it is also expressed in the testis and during osteoclastogenesis (28, 29). A role for Pou4f1 has not previously been investigated in monocyte/macrophages. We demonstrated that TGF-β1 stimulation rapidly induces Pou4f1 expression in BMDMs and that this could be prevented via blocking Smad3 or Src, known factors in the MMT response. Consistent with this finding, a conserved Smad3 binding site was identified in the promoter region of the Pou4f1 gene. TGF-β1 enriched the direct binding of Smad3 to the Pou4f1 promoter in BMDMs, and mutation analysis of the promoter validated that TGF-β1 induces Pou4f1 gene transcription in a Smad3-dependent fashion in BMDMs. Together, these findings demonstrate that Pou4f1 is a direct Smad3 target gene in TGF-β1-induced MMT in BMDMs.

Interestingly, we observed that Pou4f1 expression peaked in the early phase of fibrogenesis on day 5 in the UUO model in vivo and was rapidly and transiently induced in BMDMs in TGF-β1-driven MMT in vitro. Pou4f1 expression was closely associated with the induction of myofibroblast marker α-SMA and preceded the peak of collagen I production in vivo and in vitro, consistent with a role in the MMT process. We identified a marked up-regulation of Pou4f1 mRNA and protein in two independent models of renal fibrosis, UUO and IRI, with Pou4f1 expression localized to interstitial cells in areas of active fibrosis by immunohistochemistry. Consistent with the in vitro studies, Pou4f1 expression in the UUO model was abrogated in Smad3-KO mice which we have previously shown to be protected from the development of MMT and renal fibrosis (14). In the UUO and IRI models performed in wild-type mice, confocal microscopy and flow cytometry identified Pou4f1 expression by F4/80$^+$ macrophages and by α-SMA$^+$F4/80$^+$ MMT cells in these fibrosing kidneys. Importantly, Pou4f1 was expressed by the majority of MMT cells in human biopsy tissues, where Pou4f1 macrophages accumulated in active fibrotic lesions in chronic allograft nephropathy and significantly correlated with the degree of MMT in human kidney disease. Our findings uncovered a role of Pou4f1 in macrophages in MMT-driven renal fibrosis.

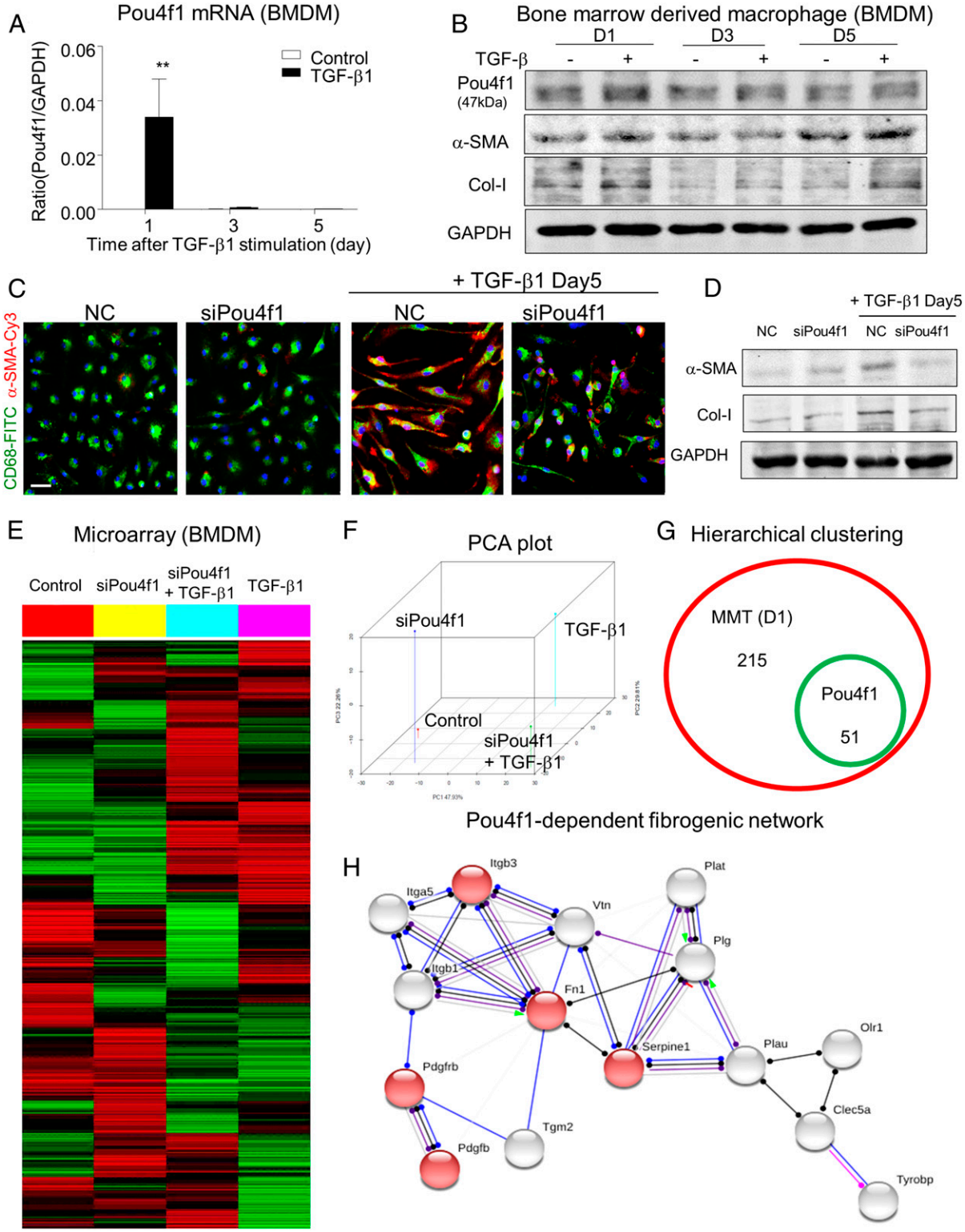

Fig. 5. A Pou4f1-dependent fibrogenic gene network at an early stage of MMT. (*A*) TGF-β1 (5 ng/mL) induced Pou4f1 transcription in BMDM at day 1 which rapidly declined to baseline as shown by real-time PCR. (*B*) Western blot shows a peak of Pou4f1 protein expression on day 1 after TGF-β1 stimulation of BMDMs which preceded the peak expression of fibrosis markers α-SMA and collagen I on day 5. siRNA-mediated silencing of Pou4f1 (siPou4f1) inhibited TGF-β1-driven MMT on day 5 in BMDMs compared to the nonsense siRNA control (NC) in terms of (*C*) a reduction in α-SMA^{+}CD68^{+} MMT cells via immunofluorescence microscopy, and (*D*) a reduction in the fibrosis markers α-SMA and collagen I via Western blotting. For microarray analysis, siPou4f1 or NC treated BMDMs, with or without TGF-β1 stimulation, were collected at 24 h. The transcriptome similarity was clearly distinguishable in each group containing a pool of three independent replicates shown by (*E*) heatmap, and (*F*) a 3D principal component analysis (PCA) plot. (*G*) A total of 215 MMT-dependent genes were identified at 24 h of TGF-β1-driven MMT, whereas 51 genes were regulated in a Pou4f1-dependent fashion in BMDMs as shown in the Venn diagram. (*H*) The Pou4f1-dependent genes formed a regulatory network containing a number of fibrogenic effectors (red) by STRING network analysis. Data represent three independent in vitro experiments. (*A*) $^{**}P < 0.01$ vs. control. (Scale bars, 20 μm.)

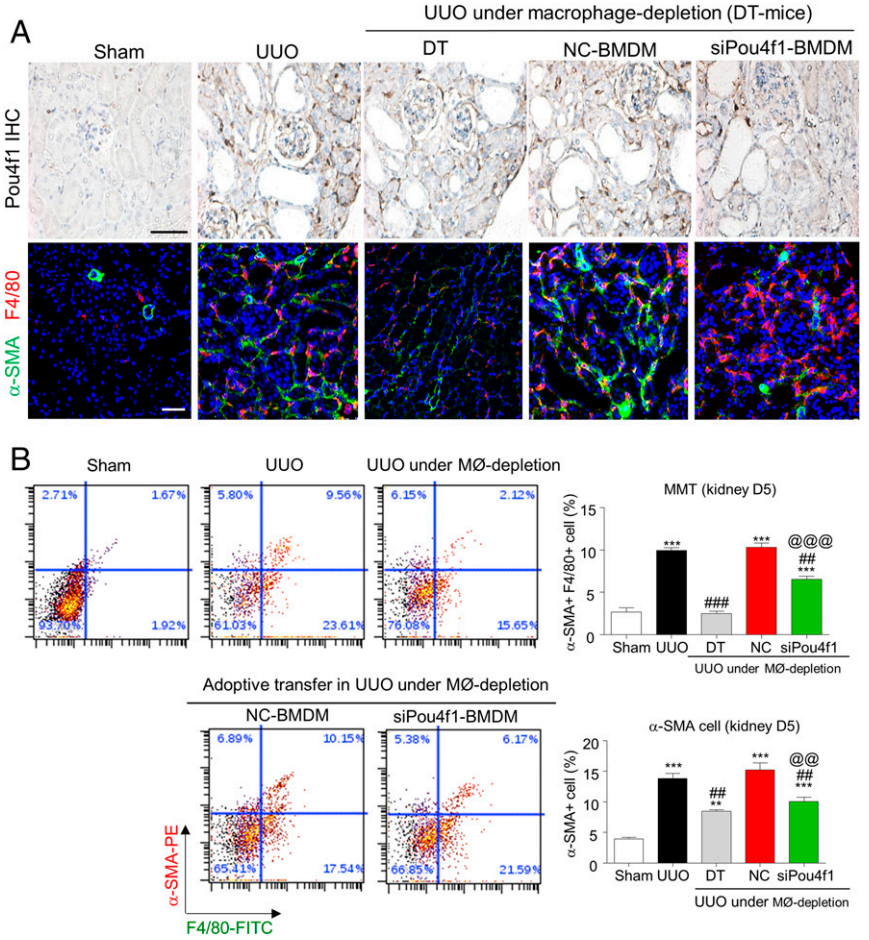

Fig. 6. Silencing of Pou4f1 in BMDM inhibits MMT in an adoptive transfer version of the UUO model. A day 5 UUO model was performed in LysM-Cre/DTR mice. Mice were treated with diptheria toxin (DT) for 3 d before UUO surgery to deplete macrophages. At 6 h after UUO surgery, mice were injected with either Pou4f1-knockdown (siPou4f1) or nonsense siRNA-treated (NC) BMDMs (2×10^6 cells/mouse) which had a 24-h stimulation with TGF-β1 (5 ng/mL) in culture prior to injection. (*A*) Immunostaining for Pou4f1 (*Upper*) and confocal microscopy for α-SMA (green) and F4/80 (red) (power panel), show that compared to the UUO control, DT treatment depleted both F4/80$^+$ macrophages and Pou4f1$^+$ interstitial cells. Both populations were restored by adoptive transfer with NC-BMDMs, while transfer of siPou4f1-BMDMs restored the F4/80$^+$ macrophage population but not the interstitial Pou4f1$^+$ cells on day 5 UUO. (*B*) Flow cytometry analysis shows that DT-induced macrophage depletion reduced both the total α-SMA$^+$ myofibroblast population and SMA$^+$CD68$^+$ MMT cells. While NC-BMDM transfer restored both of these populations, the transfer of siPou4f1-BMDMs failed to achieve this. Data represent results from six mice/group. $^{**}P < 0.01$, $^{***}P < 0.001$ vs. sham control; $^{\#\#}P < 0.01$, $^{\#\#\#}P < 0.001$ vs. UUO; $^{@@}P < 0.01$, $^{@@@}P < 0.001$ vs. adoptive transfer of NC-BMDMs under macrophage depletion (NC-BMDM). (Scale bars, 50 μm.)

A functional role for Pou4f1 in the MMT process was established in BMDMs. In vitro, silencing of Pou4f1 prevented the dramatic transformation of TGF-β1-stimulated BMDMs into myofibroblasts characterized by a highly elongated morphology with α-SMA expression and up-regulation of collagen I production. When Pou4f1-silenced BMDMs were transferred into macrophage-depleted mice, they restored the prominent kidney macrophage infiltration in both UUO and IRI models, but failed to undergo MMT, resulting in an inability to restore the α-SMA$^+$ myofibroblast population and the degree of renal fibrosis compared to the mice receiving control BMDMs. Importantly, Pou4f1 silencing did not affect the ability of BMDMs to be recruited into the injured kidney and establish a substantial infiltrate; however, Pou4f1 deletion prevented the MMT response. Whether these Pou4f1-silenced macrophages exhibit differences in polarization and function beyond the MMT response has not been investigated but would be a topic of interest for future studies. In addition, a limitation of this study is that the UUO and unilateral IRI models do not develop renal function impairment.

Mechanistically, using unbiased network analysis of the 51 Pou4f1-dependent differentially regulated genes, we identified a Serpine1-centric gene network in the TGF-β1/Smad3/Pou4f1 axis in BMDMs undergoing MMT. This is consistent with an established role for Serpine1 in renal fibrosis (30) and a recent study showing that Serpine1 deletion in fibroblasts reduces renal fibrosis in the UUO model (31). In addition, our microarray data found up-regulation of Pdgfb, Pdgfrb, and integrins in TGF-β-stimulated BMDMs. This is consistent with the MMT process and with previous studies showing that macrophages are a source of profibrogenic factors that can promote myofibroblast transition from perivascular cells in the injured kidney (32). Thus, while Pou4f1 can stimulate renal fibrosis directly through MMT, it may also be the case that Pou4f1 can indirectly promote renal fibrosis by inducing macrophage production of profibrotic factors. In mouse disease models and in human kidney disease, a small population of interstitial Pou4f1$^+$ cells do not colocalize with macrophage markers. The precise nature of these interstitial, nonmacrophage Pou4f1$^+$ cells is not clear at present. Future studies will investigate the nature of these nonmacrophage Pou4f1$^+$ interstitial cells and examine whether Pou4f1-dependent MMT plays a role in fibrotic diseases in other organs (e.g., liver, heart).

The findings in the current study are consistent with our previous investigation of MMT in human kidney disease and lineage tracing studies in bone marrow and myeloid lineages in

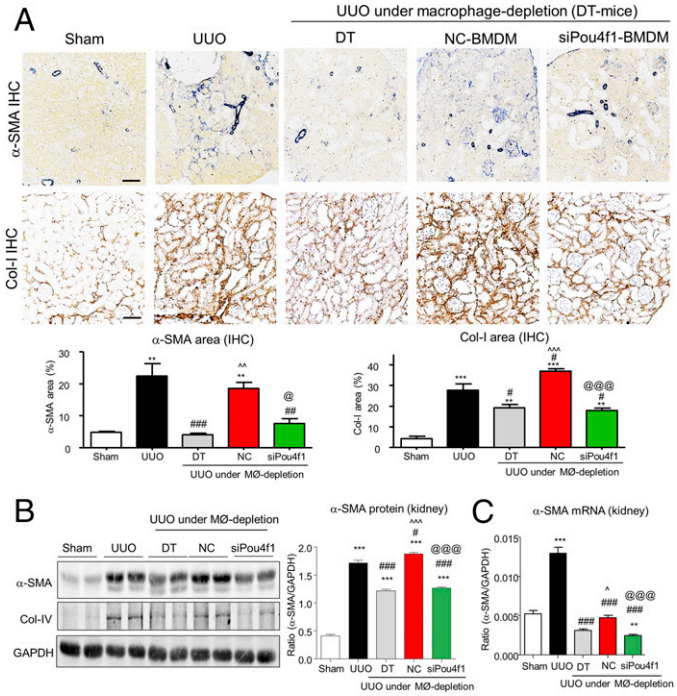

Fig. 7. Silencing of Pou4f1 in BMDMs inhibits renal fibrosis in an adoptive transfer version of the UUO model. (*A*) Immunohistochemistry staining of α-SMA and collagen I in the adoptive transfer day 5 UUO model in macrophage-depleted LysM-Cre/DTR mice. Macrophage depletion with DT reduced both α-SMA and Col-I staining in the UUO kidney. This was restored by adoptive transfer with nonsense siRNA treated (NC) BMDMs, whereas transfer of Pou4f1 siRNA-treated (siPou4f1) BMDMs failed to restore renal fibrosis. These findings were confirmed by (*B*) Western blot and (*C*) real-time PCR, for α-SMA and Col-I. Data represent results from six mice/group. $^{**}P < 0.01$, $^{***}P < 0.001$ vs. sham control; $^{\#}P < 0.05$, $^{\#\#\#}P < 0.001$ vs. UUO; $^{\wedge}P < 0.01$, $^{\wedge\wedge}P < 0.001$, $^{\wedge\wedge\wedge}P < 0.001$ vs. macrophage depletion (DT); $^{@}P < 0.05$, $^{@@@}P < 0.001$ vs. adoptive transfer of NC-BMDM under macrophage depletion (NC-BMDM). (Scale bars, 50 μm.)

experimental kidney disease (12–14). This is supported by studies from other groups showing that labeled bone marrow cells transition into α-SMA$^+$ myofibroblasts in models of renal fibrosis (3, 7, 8, 16–18). In particular, our findings are supported by studies in which conditional knockout of the collagen I gene in CD45$^+$ leukocytes substantially reduced renal fibrosis, including collagen I deposition, in the UUO model kidney by 60% (33), noting that macrophages account for ∼80% of CD45$^+$ leukocytes in the UUO kidney (34). However, it is important to acknowledge that other cell types, including renal mesenchymal cells, are also important sources of myofibroblasts during renal fibrosis. Indeed, the MMT process is somewhat controversial, given that MMT has not been identified in all studies of renal fibrosis, including a myeloid lineage tracing study (35), and a parabiosis study using single-cell RNA-seq which found that bone marrow-derived myofibroblasts contributed only around 10% of the total α-SMA$^+$ myofibroblast population in the UUO model (36). This discrepancy may in part be due to the nature and stage of disease as well as the severity of renal fibrosis; the MMT process is dynamic and can only be observed in kidney disease with active and progressive fibrosis, but is rare in diseases with acute inflammation or with nonprogressive or inactive fibrosis (13).

Taken together, our findings uncovered a crucial role of neural transcription factor Pou4f1 in TGF-β1/Smad3-driven renal fibrosis via promoting MMT. Silencing of Pou4f1 effectively blocked MMT-driven tissue fibrosis in vitro and in vivo. Thus, Pou4f1 is a specific regulator of TGF-β1/Smad3-mediated MMT and may represent a therapeutic target to prevent end-stage renal disease.

Materials and Methods

Bone Marrow-Derived Macrophages. Bone marrow cells were isolated from Smad3 WT or KO C57BL/6J mice by flushing the femur and tibia with Dulbecco's modified Eagle medium (DMEM)/F12 medium as described previously (24, 26). Cell suspensions were transferred into a new culture flask the next day to avoid fibroblast contamination and then differentiated into macrophages by a 5-d stimulation in DMEM/F12 containing 10% fetal bovine serum (FBS) and 10 ng/mL macrophage colony-stimulating factor. After this, MMT was triggered on the second passage of BMDMs by TGF-β1 (5 ng/mL) stimulation in DMEM/F12 containing 1% FBS. MMT-derived myofibroblasts on day 5 after TGF-β1 stimulation were identified by flow cytometry based on coexpression of macrophage (CD68) and myofibroblast (α-SMA) markers.

Histopathology and Immunohistochemistry. Samples of kidney nephrectomy tissue were obtained from patients with end-stage renal disease ($n = 4$), chronic allograft dysfunction ($n = 3$), and biopsies of diabetic kidney disease (one case each of stages IIa, III, and IV) and a control case of minimal change disease (Dataset 1) were obtained from the Department of Surgery (Prince of Wales Hospital, Hong Kong) and the Department of Nephrology (Tongji Hospital, Shanghai) following a protocol approved by the Clinical Research Ethics Committee. Patient samples were deidentified prior to use in this study. Human tissues and mouse kidney samples were fixed in formalin and paraffin embedded. Sections were stained with Masson's trichrome as previously described (37, 38). In addition, immunohistochemistry was performed on formalin-fixed tissue sections using a microwave-based antigen retrieval method. The primary antibodies used in this study included: Pou4f1 (sc-8429, Santa Cruz), α-SMA (A5691, Sigma), and Col-I, (1310-01, Southern Biotech). Results were imaged with a Nikon Ni-u Light Microscope.

Immunofluorescence and Opal Multiplex Immunohistochemistry. Immunostaining was performed on cultured BMDMs and frozen sections of human and mouse tissues were fixed in 2% paraformaldehyde following a previously described protocol (22, 23). In brief, sections were labeled overnight with various combinations of directly conjugated primary antibodies as follows: fluorescein isothiocyanate (FITC)-conjugated anti-CD68 antibody (bs-0649R-FITC, Bioss), FITC-conjugated anti-F4/80 (11-4801-81, eBioscience), Cy3-conjugated α-SMA antibody (C6198, Sigma), or Pou4f1 (sc-8429, Santa Cruz) conjugated with Pacific Blue (P30013, Invitrogen) or PE-conjugated Pou4f1 (sc-8429 PE, Santa Cruz). Sections were washed and, in some cases, DNA was counterstained

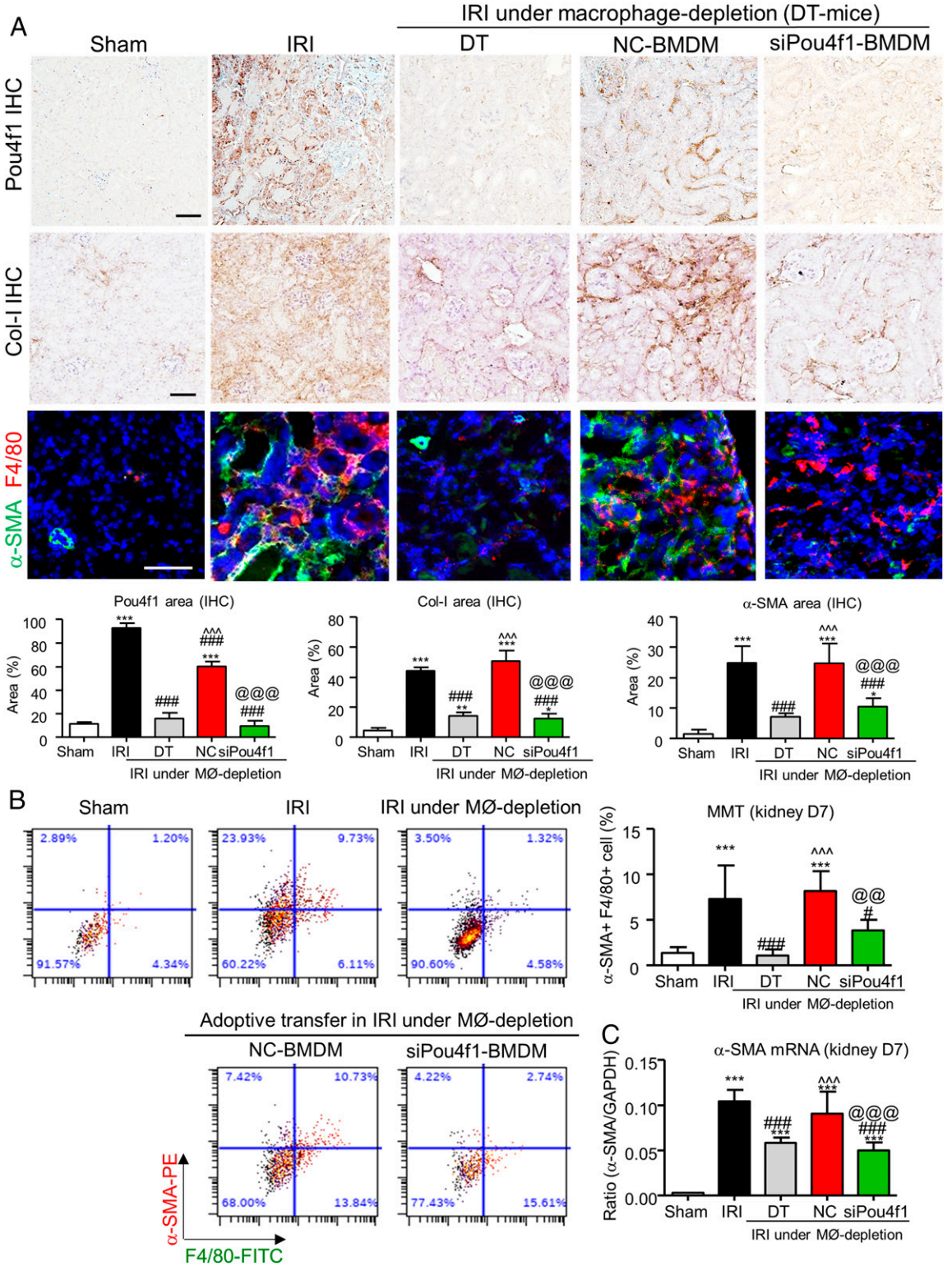

Fig. 8. Silencing of Pou4f1 in BMDMs inhibits MMT in an adoptive transfer version of the IRI model. A day 7 IRI model was performed in LysM-Cre/DTR mice. Mice were treated with DT for 3 d before IRI surgery to deplete macrophages. At 24 h after IRI surgery, mice were injected with either Pou4f1-knockdown (siPou4f1) or nonsense siRNA treated (NC) BMDM (2×10^6 cells/mouse) which had a 24-h stimulation with TGF-β1 (5 ng/mL) in culture prior to injection. (*A*) Immunohistochemistry staining for Pou4f1 (*Upper*) and Col-I (*Middle*), and confocal microscopy for α-SMA (green) and F4/80 (red) (power panel). Compared to the IRI control, DT treatment reduced F4/80$^+$ macrophages, α-SMA$^+$ myofibroblasts, Pou4f1$^+$ interstitial cells, and interstitial collagen I deposition. Adoptive transfer of NC-BMDMs restored all of these populations and collagen I deposition in the IRI model. However, transfer of siPou4f1-BMDMs restored only the F4/80$^+$ macrophage population. (*B*) Flow cytometry analysis, and (*C*) real-time PCR show that DT-induced macrophage depletion reduced both total α-SMA expression and α-SMA$^+$CD68$^+$ MMT cells. Transfer of NC-BMDMs, but not siPou4f1-BMDMs, restored both α-SMA expression and α-SMA$^+$CD68$^+$ MMT cells. Data represent results of six mice/group. $^*P < 0.05$, $^{**}P < 0.01$, $^{***}P < 0.001$ vs. sham control; $^{\#}P < 0.05$, $^{\#\#\#}P < 0.001$ vs. IRI; $^{\wedge\wedge\wedge}0.001$ vs. macrophage depletion (DT); $^{@@}P < 0.01$, $^{@@@}0.001$ vs. adoptive transfer of NC-BMDMs under macrophage depletion (NC-BMDM). (Scale bars, 50 μm.)

with DAPI and observed under a fluorescence microscope (Carl Zeiss Axio Observer Z1) or confocal microscope (Carl Zeiss LSM 880).

For Opal multiplex immunohistochemistry, sections of formalin-fixed paraffin-embedded (FFPE) patient kidney samples were deparaffinized and rehydrated, followed by endogenous horseradish peroxidase blocking and heat-induced epitope retrieval in citrate buffer. After incubation with primary antibody overnight (4 °C), the fluorescence was developed using the OPAL 4-color IHC kit (Perkin-Elmer) according to the manufacturer's protocol. Samples were imaged (four to six different areas from each sample) on the Mantra quantitative pathology workstation (Perkin-Elmer) and analyzed by inForm image analysis software (Perkin-Elmer). The area stained for MMT cells ($CD68^+\alpha$-SMA^+ cells) and Pou4f1 in the human tissue samples was normalized based on the total tissue area in each image (removing the substantial empty areas within tubular lumens and within vessels). The 3D imagining was conducted on a confocal microscope (Carl Zeiss LSM 880).

Three-Color Flow Cytometry Analysis. Cultured cells were collected on day 5 after TGF-β1 stimulation and fixed by IC Fixation Buffer (eBioscience). Single-cell suspensions were prepared from kidney tissue in one case of chronic allograft nephropathy and from mouse kidneys by digestion with Blendzyme 4 (Roche) and fixed by IC Fixation Buffer (eBioscience) for 30 min as previously described (26). The fixed cells were stained with FITC-conjugated mouse F4/80 antibody (11-4801-85, eBioscience) or FITC-conjugated human CD68 antibody (F7135, Dako), PE-conjugated α-SMA (IC1420P, R&D), and Pou4f1 (sc-8429, Santa Cruz) directly conjugated with allophycocyanin/Cy5.5 (764-0030, Innova) as in our previous protocol (39). The stained cells were washed by phosphate-buffered saline twice and then measured by FACS Caibur flow cytometer (BD Biosciences). The data were analyzed by Cytobank platform (40).

siRNA Knockdown. The nonsense siRNA control (siN05815122147, RIBOBIO) and siRNA against Pou4f1 (sense 5′-UUCAUCGUGUGGUACGUGG-3′; antisense 5′-CCACGUACCACACGAUGAA-3′) (41) were transfected into BMDMs with Lipofectamine RNAiMAX (13778075, Invitrogen) at 50 nM concentration on day −1 and day 2 of TGF-β1 (5 ng/mL) (240-B, R&D) stimulation following the procedures as described previously (24, 39). Cells were collected at different times for analysis.

Microarray Analysis. The NC- or siPou4f1-treated BMDMs (control and siPou4f1 groups) were stimulated with 5 ng/mL of TGF-β1 for 1 d (TGF-β1 and siPou4f1$^+$TGF-β1 groups), then preserved in TRIzol and submitted for microarray analysis ($n = 3$ for each condition). RNA extraction and microarray analysis were conducted with Affymetrix GeneChip Mouse Gene 2.1 ST Array by CapitalBio Technology. Pou4f1-dependent genes associated with TGF-β1-driven MMT were extracted by comparing the differentially expressed genes in the following strategy: (TGF vs. control) vs. (siPou4f1$^+$TGF vs. siPou4f1).

Real-Time PCR. Total RNA from the cultured macrophages and from mouse kidney samples was isolated by using TRIzol reagent (Life Technologies) according to the manufacturer's instructions, and quantified by using ND-2000 Nanodrop (Thermo Scientific). Total RNA (1 μg) was used to synthesize the first strand of cDNA as described previously (14). Relative mRNA expression was measured using the iQTM SYBR Green Supremix on Opticon2 system (Bio-Rad). All primers used have been described previously (24), except for Pou4f1 (42): forward 5′-GAGGCCTATTTTGCCGTACA-3′; reverse 5′-TTTCAT CCGCTTCTGCTTCT-3′. The relative expression levels of target genes were normalized with GAPDH and calculated using the $2^{-\Delta\Delta Ct}$ method.

ChIP. BMDMs were treated with 5 ng/mL TGF-β1 for 2 h, then ChIP assay was conducted using the SimpleChIP Enzymatic Chromatin IP Kit (Magnetic Beads) (Cell Signaling No. 9003) according to the manufacturer's instructions as previously described (24). In brief, immunoprecipitation was performed with the antibody against Smad3 (1:100) and irrelevant IgG was used as a control (Cell Signaling No. 9523 and No. 3900). Precipitated DNAs were identified by real-time PCR using specific primers that targeting the predicted Smad3 binding site on the conserved region of mouse Pou4f1 promoter: forward 5′-AGAAATGCGCTGTGGATGAT and reverse 5′-TCCCGA GTAGAAAGCACACA.

Western Blot Analysis. Proteins in mouse kidney tissue or in BMDMs were extracted by chilled radioimmunoprecipitation assay lysis buffer (Pierce), and then examined by Western blot analysis with primary antibodies against α-SMA, collagen-I, p-Smad3, Smad3, Pou4f1 (all at 1:1,000 dilution) and glyceraldehyde 3-phosphate dehydrogenase (GAPDH) (1:10,000 dilution), followed by incubation with the corresponding IRDyeTM800-conjugated secondary antibodies (1:10000, Rockland Immunochemicals) (24). GAPDH was used as an internal control. Expression levels of the proteins were detected by using the LiCor/Odyssey infrared image system (LI-COR; Biosciences), and the band intensities were quantified with ImageJ software (version 1.48, NIH).

Mouse Kidney Fibrosis Models and BMDM Treatment. Kidney injury was induced in male Smad3-WT and Smad3-KO C57BL/6J mice at 8 wk of age (20 to 22 g body weight), or in LysM-Cre/DTR mice using our established protocols (22, 24, 26). In brief, UUO was induced by ligating the left ureter (43), and IRI was induced by bilateral kidney artery clamping for 45 min as described in our previous study (44). Macrophage depletion in LysM-Cre/DTR mice was achieved by administration of 150 ng diphtheria toxin/mouse for 3 consecutive days before UUO or IRI surgery (26). Macrophage-depleted mice received a single intravenous (i.v.) injection of 2×10^6 cells/mouse of NC-BMDMs or siPou4f1-treated BMDMs at 6 h after UUO surgery or at 24 h after IRI surgery, while macrophage-depleted mice receiving saline injection only served as controls. The injured kidneys were collected on day 5 or day 7 after UUO, or on day 7 after IRI, and compared with the sham operation controls. The experimental procedures were performed following a protocol approved by the Animal Experimentation Ethics Committee at The Chinese University of Hong Kong.

Dual-Lucifearase Assay. pcDNA3.1$^+$ plasmids expressing Smad3 full-length sequence (Smad3) and pGL3-basic reporter plasmid containing the Pou4f1 promoter sequence with (Pou4f1-promoter) or without the predicted Smad3 binding site sequence (Pou4f1-mutant) (*SI Appendix*, Fig. S6) were constructed by Biowit Technologies Ltd (43). The luciferase reporter assay was performed by Landbiology using a dual-luciferase reporter assay kit (Promega) as in our previous studies (38, 43). The empty (pGL3-basic) or Pou4f1 reporter plasmids (Pou4f1-promoter or Pou4f1-mutant) and Renilla expression plasmid (as internal control) were cotransfected into 293T cells with empty vector (pcDNA3.1), Smad3 full-length open reading frame (ORF) (Smad3) or exons 8 and 9 deleted Smad3 mutant (Smad3-mutant) expressing plasmid. Luciferase activities were measured at 48 h according to the manufacturer's instructions by the GloMax-Multi Detection System (Promega). The reporter activity was represented by the ratio of the firefly luciferase activity (M1) to the Renilla luciferase activity (M2) as M1/M2 and shown as mean ± SEM fold induction of luciferase in three independent experiments.

Statistical Analysis. Data obtained from this study are presented as the mean ± SD (SD). Statistical analyses were performed using one-way ANOVA, followed by Newman–Keuls posttest from Prism 5.0 GraphPad Software (45).

Data Availability. All relevant data are within the manuscript and its *SI Appendix* files.

ACKNOWLEDGMENTS. We thank Dr. Chuxia Deng and Dr. Stefan Frank for the Smad3$^{+/-}$ and LysM-Cre/DTR mice, respectively. This study was supported by Research Grants Council of Hong Kong (14106518, 14111019, 14111720, 14121816, 14163317, 14117418, 14104019, R4012-18, and C7018-16G); Innovation and Technology Fund of Hong Kong (ITS/068/18, PiH/009/19, PiH/010/19, PiH/394/19, InP/008/19, InP/009/19, and InP/159/19); National Health and Medical Research Council of Australia (APP1122073); The Chinese University of Hong Kong's Faculty Innovation Award (4620528); Direct Grant for Research (4054386, 4054440, and 4054510); The Guangdong-Hong Kong-Macao-Joint Labs Program from Guangdong Science and Technology (2019B121205005); and the Lui Che Woo Institute of Innovative Medicine (CARE program).

1. D. C. Rockey, P. D. Bell, J. A. Hill, Fibrosis–A common pathway to organ injury and failure. *N. Engl. J. Med.* **372**, 1138–1149 (2015).
2. F. Klingberg, B. Hinz, E. S. White, The myofibroblast matrix: Implications for tissue repair and fibrosis. *J. Pathol.* **229**, 298–309 (2013).
3. V. S. LeBleu *et al.*, Origin and function of myofibroblasts in kidney fibrosis. *Nat. Med.* **19**, 1047–1053 (2013).
4. K. Jinde *et al.*, Tubular phenotypic change in progressive tubulointerstitial fibrosis in human glomerulonephritis. *Am. J. Kidney Dis.* **38**, 761–769 (2001).
5. Y. Y. Ng *et al.*, Tubular epithelial-myofibroblast transdifferentiation in progressive tubulointerstitial fibrosis in 5/6 nephrectomized rats. *Kidney Int.* **54**, 864–876 (1998).
6. E. M. Zeisberg *et al.*, Endothelial-to-mesenchymal transition contributes to cardiac fibrosis. *Nat. Med.* **13**, 952–961 (2007).
7. M. Broekema *et al.*, Bone marrow-derived myofibroblasts contribute to the renal interstitial myofibroblast population and produce procollagen I after ischemia/reperfusion in rats. *J. Am. Soc. Nephrol.* **18**, 165–175 (2007).

8. H. S. Jang, J. I. Kim, S. J. Han, K. M. Park, Recruitment and subsequent proliferation of bone marrow-derived cells in the postischemic kidney are important to the progression of fibrosis. *Am. J. Physiol. Renal Physiol.* **306**, F1451–F1461 (2014).
9. J. Li, J. A. Deane, N. V. Campanale, J. F. Bertram, S. D. Ricardo, The contribution of bone marrow-derived cells to the development of renal interstitial fibrosis. *Stem Cells* **25**, 697–706 (2007).
10. Y. Xia, J. Yan, X. Jin, M. L. Entman, Y. Wang, The chemokine receptor CXCR6 contributes to recruitment of bone marrow-derived fibroblast precursors in renal fibrosis. *Kidney Int.* **86**, 327–337 (2014).
11. D. J. Nikolic-Paterson, S. Wang, H. Y. Lan, Macrophages promote renal fibrosis through direct and indirect mechanisms. *Kidney Int. Suppl.* **4**, 34–38 (2014).
12. Y. Y. Wang *et al*., Macrophage-to-myofibroblast transition contributes to interstitial fibrosis in chronic renal allograft injury. *J. Am. Soc. Nephrol.* **28**, 2053–2067 (2017).
13. S. Wang *et al*., TGF-β/Smad3 signalling regulates the transition of bone marrow-derived macrophages into myofibroblasts during tissue fibrosis. *Oncotarget* **7**, 8809–8822 (2016).
14. X. M. Meng *et al*., Inflammatory macrophages can transdifferentiate into myofibroblasts during renal fibrosis. *Cell Death Dis.* **7**, e2495 (2016).
15. P. M. Tang, D. J. Nikolic-Paterson, H. Y. Lan, Macrophages: Versatile players in renal inflammation and fibrosis. *Nat. Rev. Nephrol.* **15**, 144–158 (2019).
16. Y. L. Phua, N. Martel, D. J. Pennisi, M. H. Little, L. Wilkinson, Distinct sites of renal fibrosis in Crim1 mutant mice arise from multiple cellular origins. *J. Pathol.* **229**, 685–696 (2013).
17. J. Yang *et al*., Adiponectin promotes monocyte-to-fibroblast transition in renal fibrosis. *J. Am. Soc. Nephrol.* **24**, 1644–1659 (2013).
18. Y. Yang *et al*., Fate alteration of bone marrow-derived macrophages ameliorates kidney fibrosis in murine model of unilateral ureteral obstruction. *Nephrol. Dial. Transplant.* **34**, 1657–1668 (2019).
19. X. M. Meng, D. J. Nikolic-Paterson, H. Y. Lan, TGF-β: The master regulator of fibrosis. *Nat. Rev. Nephrol.* **12**, 325–338 (2016).
20. X. Yang *et al*., Targeted disruption of SMAD3 results in impaired mucosal immunity and diminished T cell responsiveness to TGF-beta. *EMBO J.* **18**, 1280–1291 (1999).
21. Q. Zhou *et al*., Identification of novel long noncoding RNAs associated with TGF-β/Smad3-mediated renal inflammation and fibrosis by RNA sequencing. *Am. J. Pathol.* **184**, 409–417 (2014).
22. M. Feng *et al*., TGF-β mediates renal fibrosis via the Smad3-Erbb4-IR long noncoding RNA axis. *Mol. Ther.* **26**, 148–161 (2018).
23. S. F. Sun *et al*., Novel lncRNA Erbb4-IR promotes diabetic kidney injury in *db/db* mice by targeting miR-29b. *Diabetes* **67**, 731–744 (2018).
24. P. M. Tang *et al*., The proto-oncogene tyrosine protein kinase Src is essential for macrophage-myofibroblast transition during renal scarring. *Kidney Int.* **93**, 173–187 (2018).
25. E. J. Huang *et al*., Brn3a is a transcriptional regulator of soma size, target field innervation and axon pathfinding of inner ear sensory neurons. *Development* **128**, 2421–2432 (2001).
26. L. L. Lv *et al*., The pattern recognition receptor, Mincle, is essential for maintaining the M1 macrophage phenotype in acute renal inflammation. *Kidney Int.* **91**, 587–602 (2017).
27. M. B. Lodish, Clinical review: Kinase inhibitors: Adverse effects related to the endocrine system. *J. Clin. Endocrinol. Metab.* **98**, 1333–1342 (2013).
28. V. Budhram-Mahadeo *et al*., The closely related POU family transcription factors Brn-3a and Brn-3b are expressed in distinct cell types in the testis. *Int. J. Biochem. Cell Biol.* **33**, 1027–1039 (2001).
29. U. Schulze-Späte *et al*., Brn3 transcription factors control terminal osteoclastogenesis. *J. Cell. Biochem.* **102**, 1–12 (2007).
30. A. K. Ghosh, D. E. Vaughan, PAI-1 in tissue fibrosis. *J. Cell. Physiol.* **227**, 493–507 (2012).
31. L. Yao *et al*., Fibroblast-specific plasminogen activator inhibitor-1 depletion ameliorates renal interstitial fibrosis after unilateral ureteral obstruction. *Nephrol. Dial. Transplant.* **34**, 2042–2050 (2019).
32. H. M. Perry *et al*., Perivascular $CD73^+$ cells attenuate inflammation and interstitial fibrosis in the kidney microenvironment. *Am. J. Physiol. Renal Physiol.* **317**, F658–F669 (2019).
33. S. Buchtler *et al*., Cellular origin and functional relevance of collagen I production in the kidney. *J. Am. Soc. Nephrol.* **29**, 1859–1873 (2018).
34. Y. Le Meur *et al*., Macrophage accumulation at a site of renal inflammation is dependent on the M-CSF/c-fms pathway. *J. Leukoc. Biol.* **72**, 530–537 (2002).
35. I. G. Gomez, J. S. Duffield, The FOXD1 lineage of kidney perivascular cells and myofibroblasts: Functions and responses to injury. *Kidney Int. Suppl.* **4**, 26–33 (2014).
36. R. Kramann *et al*., Parabiosis and single-cell RNA sequencing reveal a limited contribution of monocytes to myofibroblasts in kidney fibrosis. *JCI Insight* **3**, e99561 (2018).
37. Q. M. Wang *et al*., Enhanced cancer immunotherapy with Smad3-silenced NK-92 cells. *Cancer Immunol. Res.* **6**, 965–977 (2018).
38. Y. Y. Zhang *et al*., LRNA9884, a novel Smad3-dependent long noncoding RNA, promotes diabetic kidney injury in *db/db* mice via enhancing MCP-1-dependent renal inflammation. *Diabetes* **68**, 1485–1498 (2019).
39. P. M. Tang *et al*., A novel feeder-free system for mass production of murine natural killer cells in vitro. *J. Vis. Exp.*, 56785 (2018).
40. T. J. Chen, N. Kotecha, Cytobank: Providing an analytics platform for community cytometry data analysis and collaboration. *Curr. Top. Microbiol. Immunol.* **377**, 127–157 (2014).
41. T. Hohenauer *et al*., The neural crest transcription factor Brn3a is expressed in melanoma and required for cell cycle progression and survival. *EMBO Mol. Med.* **5**, 919–934 (2013).
42. H. Cwerman-Thibault *et al*., Neuroglobin can prevent or reverse glaucomatous progression in DBA/2J mice. *Mol. Ther. Methods Clin. Dev.* **5**, 200–220 (2017).
43. P. M. Tang *et al*., Smad3 promotes cancer progression by inhibiting E4BP4-mediated NK cell development. *Nat. Commun.* **8**, 14677 (2017).
44. J. H. Li *et al*., Macrophage migration inhibitory factor promotes renal injury induced by ischemic reperfusion. *J. Cell. Mol. Med.* **23**, 3867–3877 (2019).
45. C. Li *et al*., The Mincle/Syk/NF-κB Signaling Circuit Is Essential for Maintaining the Protumoral Activities of Tumor-Associated Macrophages. *Cancer Immunol Res*, 10.1158/2326-6066.CIR-19-0782 (2020).